Organic & Biomolecular Chemistry

Cite this: *Org. Biomol. Chem.*, 2012, **10**, 2044

www.rsc.org/obc

PAPER

Fungal biofilm inhibitors from a human oral microbiome-derived bacterium†

Xiaoru Wang,‡[a] Lin Du,‡[a] Jianlan You,[a] Jarrod B. King[a] and Robert H. Cichewicz*[a,b]

Received 3rd November 2011, Accepted 21st December 2011
DOI: 10.1039/c2ob06856g

The human mouth is home to a rich assortment of native and transient microorganisms. One of the commonly encountered bacterial species, *Streptococcus mutans*, was shown to generate the novel hybrid polyketide-nonribosomal peptide metabolite mutanobactin A (**1**). We have characterized three new analogues, mutanobactins B-D (**2–4**), and subjected these compounds to further biomedical evaluation. Metabolites **1**, **2**, and **4** were found to inhibit biofilm formation by the fungal oral-pathogen *Candida albicans*. Compound **4** was the most potent metabolite with an IC_{50} value of 5.3 ± 0.9 μM. Using a combination of Marfey's analysis, proton spin–spin coupling, and ^{1}H-^{1}H NOESY data, we proposed absolute configuration assignments *in toto* for **1–3** and a partial assignment for **4**. In addition, feeding studies with isotopically labeled precursor metabolites (acetate and amino acids) have helped to determine the biosynthetic origins of this unique natural product family.

Introduction

An average adult human mouth has a surface area of only ~215 cm^2,[1] yet it is home to an amazingly large and diversified assemblage of microbial species.[2–6] It is estimated that in excess of 1.9×10^4 bacterial phylotypes occupy the mouth[7] forming a complex community that is dominated by Firmicutes, Proteobacteria, Bacteroidetes, Actinobacteria, and Fusobacteria.[8] Certain fungi including *Candida* spp. also reside in the mouth, although these microbes tend to be numerically less abundant in healthy adults.[9]

Streptococcus mutans is one of the perennial members of the oral microbial community.[10,11] Substantial interest in this microbe has evolved due in part to its ubiquity, as well as evidence linking *S. mutans* to the development of dental caries.[12–14] However, recent studies using cultivation-dependent[15] and culture-independent[16] screening techniques of caries-associated microbial assemblages have called some of these assertions into question. Regardless, *S. mutans* is an important component of the oral microbial community due in part to its assorted interactions with other bacteria,[14] fungi,[17,18] and mammalian cells.[19,20]

Although there is an abundance of published reports illustrating the extent to which bacteria and fungi are capable of interacting with other microorganisms within their vicinity,[21–23] the majority of biomolecules responsible for influencing these biological processes remain unknown. Small-molecule signals are thought to play vital roles in the intraspecies and interspecies interactions involving microbiome bacteria and humans[24–26] and our group has taken an active role pursuing the identities of these chemical agents. We had previously reported that *S. mutans* UA159 generated the unique secondary metabolite mutanobactin A (**1**),[27] which inhibited the morphological switch of pathogenic *Candida albicans* from a yeast to a filamentous morphology.[28] Several questions emerged from that study that included 1) what is the absolute configuration of all the stereogenic centers in **1**, 2) what are the biosynthetic precursors that contribute to building this polyketide-non-ribosomal-peptide molecule, and 3) what are the structures of the analogues of **1**? In this study, we have addressed each of these issues, as well as examined the biological impact of mutanobactins on the ability of pathogenic *C. albicans* to form biofilms. The formation of biofilms by *Candida* spp. is a topic of significant medical relevance[29] because biofilms serve as reservoirs for antibiotic-resistant persister cells, which are key factors in the development of therapeutically-recalcitrant and life-threatening yeast infections.[30,31]

Results and discussion

A sample taken from the ethyl-acetate-soluble material obtained from partitioning 40 L of *S. mutans* UA159 culture was analyzed by reversed-phase LC-ESIMS (positive mode). This revealed a group of three new peaks with retention times and mass-to-

[a]*Natural Products Discovery Group, Department of Chemistry and Biochemistry, Stephenson Life Sciences Research Center, 101 Stephenson Parkway, University of Oklahoma, Norman, OK73019, USA. E-mail: rhcichewicz@ou.edu; Tel: +1 (405) 325-6969*
[b]*Graduate Program in Ecology and Evolutionary Biology, University of Oklahoma, Norman, OK73019, USA*

†Electronic supplementary information (ESI) available: MS, IR, and NMR (^{1}H, ^{13}C, ^{1}H-^{1}H COSY, ^{1}H-^{1}H TOCSY, ^{1}H-^{1}H NOESY, ^{1}H-^{13}C HSQC, and ^{1}H-^{13}C HMBC) data for **2**, **3**, and **4** and additional data described in this manuscript. See DOI: 10.1039/c2ob06856g

‡These authors contributed equally to this work.

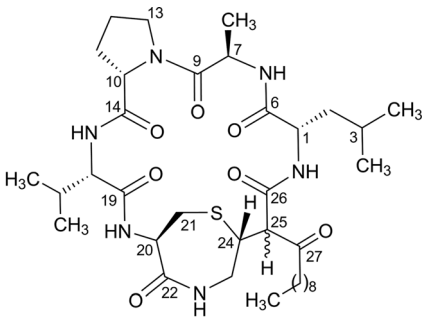

1 (25*R*)
3 (25*S*)

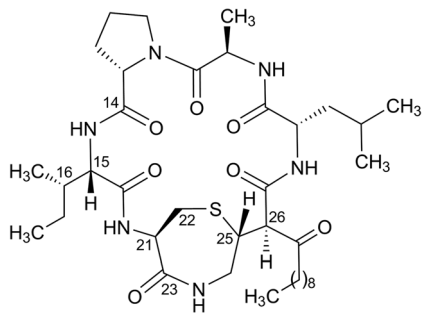

2

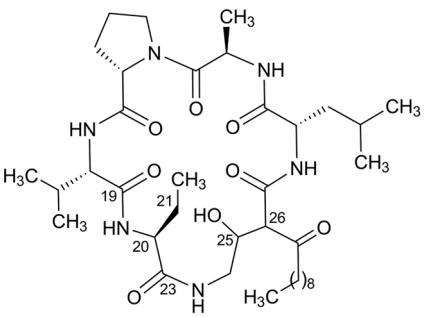

4

Fig. 1 Structures of mutanobactins A–D (**1**–**4**) from the oral microbiome bacterium *S. mutans*.

charge ratios similar to **1** (*m*/*z* 743 $[M + Na]^+$, t_R 24.6 min). The three compounds exhibited base peaks at *m*/*z* 757 $[M + Na]^+$ (t_R 25.8 min), 743 $[M + Na]^+$ (t_R 24.6 min), and 721 $[M + H]^+$ (t_R 24.9 min). In light of the substantial similarity between the LC-ESIMS properties of these compounds and **1**, we suspected that these peaks represented new mutanobactins (Fig. 1). Subsequently, these metabolites were targeted for purification and structure characterization (repeated HP20SS column chromatography and reversed-phase HPLC).

HRESIMS analysis of mutanobactin B (**2**) provided a pseudomolecular ion with *m*/*z* 757.4298 that corresponded to a molecular formula of $C_{37}H_{62}N_6O_7SNa$ ($[M + Na]^+$, calcd 757.4298) (Fig. S1†). Compared to **1**, this indicated that compound **2** possessed one additional carbon and two additional hydrogen atoms. Although the ^1H NMR data for **2** (Table 1) were nearly superimposable with those for **1**, we observed a subtle shift in the resonances appearing in the highfield region (~1.0 ppm) of the spectrum (*note*: upon further scrutiny, we have found it necessary to reassign some of the carbon and proton resonances in the hydrocarbon tail of **1**; refer to ESI Table S1, for details of these changes†). In addition, ^{13}C NMR (Table 1) revealed a new carbon resonance at δ_C 10.0 (C-18) (Fig. S3†). Using ^1H-^1H COSY and ^1H-^1H TOCSY (Fig. S6 and S7†), we traced the spin system originating from the hydrogens attached to C-18 (δ_H 0.78, H-18) to a series of protons at δ_H 8.01 (N*H*-15) 3.75 (H-15), 2.19 (H-16), 0.79 (H-19), 1.35 (H-17a), and 1.02 (H-17b), which we deduced were part of an Ile residue (Fig. 2). This was supported by the ^1H-^{13}C HSQC and ^1H-^{13}C HMBC NMR data (Fig. S4 and S5†) that confirmed the Val in **1** was replaced by an Ile in **2** (Fig. 2). Further examination revealed that all other portions of the planar structure of **2** remained unchanged relative to compound **1**.

Mutanobactin C (**3**) afforded a pseudomolecular ion at *m*/*z* 743.4138 that corresponded to a molecular formula of $C_{36}H_{60}N_6O_7SNa$ ($[M + Na]^+$, calcd 743.4142) (Fig. S10†). In addition to sharing the same molecular formula as **1**, the ^{13}C NMR data for **1** (Table S1†) and **3** (Table 1) were found to be remarkably similar. Analysis of the ^1H-^{13}C HSQC and ^1H-^{13}C HMBC data (Fig. S13 and S14†) obtained for **3** enabled us to determine that the new metabolite possessed the same planar structure as **1**. But upon closer scrutiny, several subtle changes in chemical shifts for protons H-21a/b ($\Delta = -0.20$ and 0.24 ppm), H-23a/b ($\Delta = -0.38$ and -0.07 ppm), H-24 ($\Delta = -0.19$ ppm), and H-25($\Delta = -0.19$ ppm) were observed (Table 1). Thus, it was concluded that **3** was a diastereomer of **1** with the configuration of one or more stereogenic carbons having been altered in the vicinity of the aforementioned protons.

High resolution ESIMS of mutanobactin D (**4**) revealed that this metabolite possessed a molecular formula of $C_{37}H_{64}N_6O_8Na$ ($[M + Na]^+$, *m*/*z* of 743.4681, calcd 743.4683) (Fig. S19†). The absence of the sulfur atom signified that the 1,4-thiazepan-5-one system in **1**–**3** was not present in **4**. The loss of this substructure was supported by analysis of the ^1H and ^{13}C NMR spectra (Fig. S20 and S21†) (and later verified by 2D ^1H-^1H TOCSY, ^1H-^{13}C HSQC, and ^1H-^{13}C HMBC experiments; Fig. S22, S23, and S25†), which showed that key resonances attributable to the Ile, Ala, Pro, and Val residues and hydrocarbon tail remained intact, but the 1,4-thiazepan-5-system was missing. Instead, a new spin set consisting of protons at δ_H 8.46, 3.80, 1.52 and 0.85 was detected by TOCSY (Fig. S25†) leading to the identification of an α-aminobutyric acid (Aaba) residue in **4**. A second spin set with protons at δ_H 2.65, 3.98, 3.38, and 4.70 (exchangeable) was identified that was attributed to a hydroxyglycine residue. HMBC data indicated that one of the hydroxyglycine carbons (δ_C 66.7, C-25) was attached to the C-26 methine (δ_C 61.7), which served as the junction between the C-27 (δ_C 166.3) and C-28 (δ_C 204.5) carbonyls (Fig. 2). Protons (δ_H 2.65, H-24a and 3.38, H-24b) attached to the other hydroxyglycine carbon (δ_C 42.1, C-24) exhibited $^3J_{H-C}$ coupling with the carbonyl of the adjacent Aaba residue (Fig. 2). In addition, the proton from the Aaba residue methine (δ_H 3.80, H-20) coupled ($^3J_{H-C}$) with the Ala carbonyl (Fig. 2). Therefore, the planar structure of **4** was determined to comprise a new 20-membered macrocycle.

With the planar structures of metabolites **2**–**4** established, we proceeded to investigate the absolute configuration of each

Table 1 ^{1}H (500 MHz) and ^{13}C (100 MHz) NMR data for **2–4** acquired in DMSO-d_6

	2		**3**		**4**	
Position	δ_C	δ_H, mult. (*J* in Hz)	δ_C	δ_H, mult. (*J* in Hz)	δ_C	δ_H, mult. (*J* in Hz)
1	50.3, CH	4.43 ddd (3.6, 9.3, 11.0)	50.6, CH	4.43, m	52.3, CH	4.21, m
2a	40.4, CH_2	1.44, m	40.2, CH_2	1.59, m	40.5, CH_2	1.45, m
2b		1.82, ddd (3.6, 10.5, 13.9)		1.52, m		1.71
3	24.2, CH	1.60, m	24.4, CH	1.60, m	24.5, CH	1.43, m
4	20.8, CH_3	0.82, d (6.6)	21.1, CH_3	0.84, d (6.5)	21.6, CH_3	0.91, d (6.4)
5	23.5, CH_3	0.92, d (6.4)	23.1, CH_3	0.92,d (6.5)	23.6, CH_3	0.81, d (6.4)
6	170.5, C		170.2, C		172.0, C	
7	48.1, CH	4.51, q (6.7)	47.5, CH	4.46, m	47.5, CH	4.25, m
8	17.6, CH_3	1.17, d (6.7)	16.7, CH_3	1.20, d (6.8)	15.1, CH_3	1.20, d (6.9)
9	170.0, C		171.6, C		171.1, C	
10	61.2, CH	4.11, dd (3.4, 8.7)	61.2, CH	4.17, dd (3.7, 8.7)	60.0, CH	4.35, brd (7.0)
11a	29.6, CH_2	1.70, m	29.6, CH_2	1.87, m	29.4, CH_2	1.98, m
11b		2.13, m		2.12, m		2.06, m
12a	24.5, CH_2	1.90, m	24.2, CH_2	1.90, m; 1.78, m	23.6, CH_2	1.76, m
12b						1.98, m
13a	46.8, CH_2	3.42, m	47.2, CH_2	3.51, m	46.5, CH_2	3.54, m
13b		3.68, m		3.78, m		3.91, brt (8.9)
14	171.6, C		171.1, C		170.5, C	
15	56.7, CH	3.75, dd (8.7, 10.0)	58.8, CH	3.92, t (6.6, 7.0)	58.2, CH	4.05, brt (9.9)
16	31.5, CH	2.19, m	29.2, CH	2.21, m	29.5, CH	2.13, m
17a	21.4, CH_2	1.35, m	19.7, CH_3	0.92, d (6.7)	19.8, CH_3	0.90, d (6.5)
17b		1.02, m				
18	10.0, CH_3	0.78, m	18.5, CH_3	0.93, d (6.7)	19.4, CH_3	0.97, d (6.6)
19	16.2, CH_3	0.79, d (6.8)	170.1, C		172.0, C	
20	168.9, C		56.3, CH	4.46, m	56.4, CH	3.80, td (2.4, 7.4)
21a	52.3, CH	4.85, m	26.2, CH_2	2.43, m	23.8, CH_2	1.52, m
21b				2.95, dd (9.9, 15.3)		
22a	28.4, CH_2	2.21, brd 16.3	169.8, C		10.3, CH_3	0.85, t (7.4)
22b		3.19, dd (8.2, 16.3)				
23a	170.3, C		40.7, CH_2	3.17, m	172.5, C	
23b				3.35, m		
24a	43.8, CH_2	2.76, m	41.1, CH	3.44, m	42.1, CH_2	2.65, brd (13.7)
24b		3.28, m				3.38, m
25	40.9, CH	3.25, m	62.8, CH	4.06, d (8.9)	66.7, CH	4.18, m
26	61.7, CH	3.88, d (9.4)	166.3, C		61.7, CH	3.98, d (10.4)
27	167.7, C		202.7, C		166.3, C	
28a	203.8, C		40.8, CH_2	2.37, m	204.5, C	
28b				2.43, m		
29a	41.3, CH_2	2.33, m	23.0, CH_2	1.45, m	40.1, CH_2	2.23, m
29b		2.44, dd (8.4, 11.4)				2.35, m
30	23.0, CH_2	1.45, m	28.4, CH_2	1.17, m	22.5, CH_2	1.36, m
31	28.5, CH_2	1.20, m	28.7, CH_2	1.22, m	28.4, CH_2	1.16, m
32	28.6, CH_2	1.22, m	28.9, CH_2	1.22, m	28.6, CH_2	1.20, m
33	28.9, CH_2	1.22, m	28.7, CH_2	1.22, m	29.0, CH_2	1.21, m
34	28.7, CH_2	1.23, m	31.3, CH_2	1.22, m	28.7, CH_2	1.22, m
35	31.3, CH_2	1.23, m	22.1, CH_2	1.24, m	31.2, CH_2	1.22, m
36	22.1, CH_2	1.23, m	14.0, CH_3	0.85, t (6.8)	22.1, CH_2	1.22, m
37	14.0, CH_3	0.85, t (6.8)			13.9, CH_3	0.84, t (6.8)
1-NH		8.55, d (9.1)		8.70. brs		8.12, d (4.5)
7-NH		7.74, d (6.6)		7.91, d (4.9)		9.05, brs
15-NH		8.01, d (8.3)		7.35, brs		7.63, d (9.3)
20-NH				7.74, d (6.3)		8.46, d (2.6)
21-NH		7.20, d (7.6)				
23-NH				7.69, m		
24-NH		7.93, dd (6.2, 8.2)				7.81, dd (2.5, 14.1)
25-OH						4.70, brs

compound. Several approaches were used including biogenic considerations,[27] Marfey's method,[32] proton–proton spin coupling, and ^{1}H-^{1}H NOESY. In addition, insights gained from our structure analyses of **2–4** provided a good opportunity to re-evaluate the yet undefined configuration of stereogenic centers C-20, C-24, and C-25 in **1**.[28] Numerous attempts to produce suitable crystals of **1–4** for X-ray analysis failed with gels or amorphous precipitates consistently forming.

The FDAA-derivatized hydrolysates of **2**, **3**, and **4** were analyzed by HPLC and the products compared to derivatized amino acid standards for the D and L forms of Aaba, Ala, Ile, Leu, Pro, and Val (Fig. S34†). This enabled us to confirm that compound **2** contained L-Leu, D-Ala, L-Pro, and L-Ile residues (Fig. S35†); compound **3** contained L-Leu, D-Ala, L-Pro, and L-Val residues (Fig. S36†); and compound **4** contained L-Leu, D-Ala, L-Pro, L-Val, and L-Aaba residues (Fig. S37†).

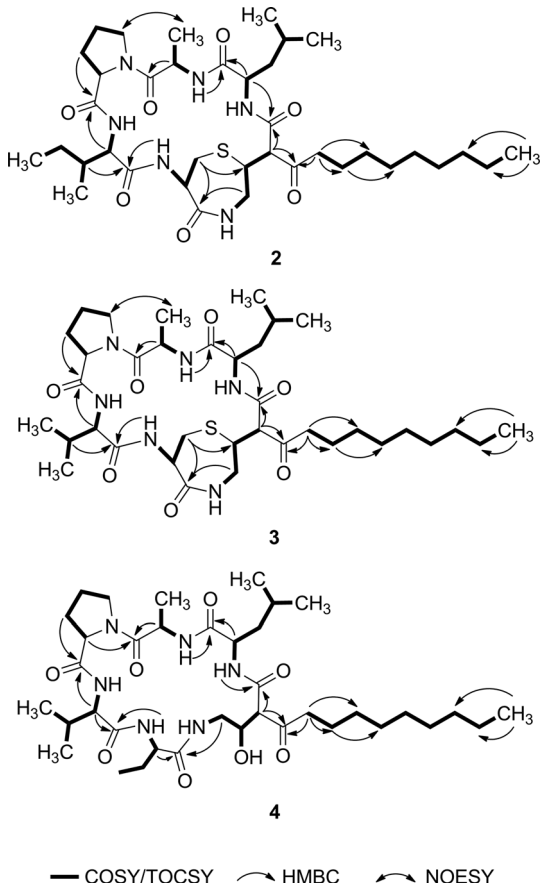

Fig. 2 Important ^{1}H-^{1}H COSY, ^{1}H-^{1}H TOCSY,^{1}H-^{13}C HMBC, and ^{1}H-^{1}H NOESY correlations used to deduce the planar structures of mutanobactins B–D (**2**–**4**).

During our previous investigation of **1**, we had performed a 2D ^{1}H-^{1}H NOESY experiment and this had provided us with a substantial number of NOE cross peaks (Fig S32†). However, the lack of additional mutanobactin congeners at that time prohibited us from confidently assigning the absolute configuration of C-22, C-24, and C-25. Now with diastereomer **3** in hand, determining the absolute configuration of each stereogenic carbon became relatively straightforward. We identified three key elements that made this analysis possible: first, both **1** and **3** exhibited large (*anti* configuration) vicinal couplings between H-24 and H-25 (J = 9.8 and J = 8.9 Hz, respectively); second, the *anti* relationships between H-24 and H-25 were further substantiated by the absence of NOE cross peaks between these protons in **1** and **3**; and third, compounds **1** and **3** exhibited dramatically different *trans*-annular NOE cross peaks between their respective 1,4-thiazepan-5-one rings and the amide protons of the D-Ala residues (Fig S17 and S32†). In the case of compound **1**, both H-21a and H-21b exhibited *trans*-annular NOE cross peaks with the D-Ala N*H* (Fig. 3). In contrast, compound **3** H-23a and H-23b produced strong NOE correlations to the D-Ala N*H* (Fig. 3). These data provided compelling evidence that the 1,4-thiazepan-5-one system was rotated roughly 180° in **3** relative to **1**. Accordingly, we determined that **1** possessed a 24*R**,25*R** relative configuration and **3** had a 24*R**,25*S** relative configuration.

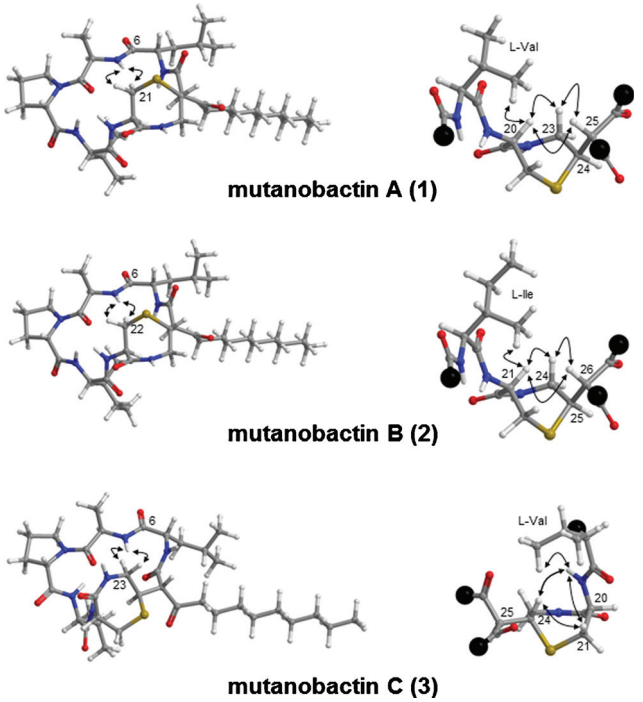

Fig. 3 Key ^{1}H-^{1}H NOESY correlations observed for **1**–**3**. For each compound, *trans*-annular NOE correlations from the 1,4-thiazepan-5-one rings to the amid D-Ala 7-N*H* are shown on the left side of the figure. On the right, close-up views are shown of the NOE correlations involving other 1,4-thiazepan-5-one ring protons. The black spheres represent places that the molecule was truncated for this figure.

Further support for this hypothesis was obtained *via* computer-generated lowest energy calculations performed on **1** and **3** using a MM2 force field parameter set. In addition to delivering *in silico* validation of the configuration assignments, we observed striking differences in the predicted orientations of the Cys residue α-protons in **1** and **3** (Fig. 3). This was supported by spectroscopic data in which Cys H-20 of **1** produced NOE cross peaks with the 1,4-thiazepan-5-one ring protons H-23 and H-25, as well as L-Val H-17/H-18. In contrast, inversion of the 1,4-thiazepan-5-one ring in **3** resulted in Cys H-20 adopting a pseudoequatorial orientation (Fig. 3). This led to the absence of NOE cross peaks between Cys H-20 and H-23/H-25. Taking into account the configuration assignments for C-24/C-25, the NOE cross peaks involving the C-20 methine protons, NOESY data between protons within the 1,4-thiazepan-5-one ring and the surrounding amino acid residues, as well as the *trans*-annular NOE correlations (Fig. 3), we refined the absolute configuration of **1** as 1*S*,7*R*,10*S*,15*S*,20*R*,24*R*,25*R* and its C-25 epimer **3** as 1*S*,7*R*,10*S*,15*S*,20*R*,24*R*,25*S*.

Metabolite **2** provided 2D ^{1}H-^{1}H NOESY data that were nearly identical with those afforded by **1** (Fig S8†). In light of the significant similarities between these compounds, **2** was deduced as having a 1*S*,7*R*,10*S*,15*S*,16*S*,21*R*,25*R*,26*R* absolute configuration. Data obtained from NOESY and long-range $^{2\text{–}3}J_{\text{H–C}}$ experiments with **4** proved inconclusive for discerning the absolute configuration of C-25 and C-26. However, results from the Marfey's experiment (*vide supra*) enabled us to deduce the absolute configuration of the other stereogenic carbons as 1*S*,7*R*,10*S*,15*S*,20*S* (Fig S37†).

Table 2 Enrichment ratios and ^{13}C–^{13}C, ^{15}N–^{13}C couplings (J(C, C)) for isotope feeding experiments with **1**

Position	δ_C[a]	[1-^{13}C] acetate ER[b]	[2-^{13}C] acetate ER	[^{15}N,$^{13}C_2$]glycine ^1J (C–C, N–C) (Hz)
22	170.4	1.6	1.0	
23	43.7	1.5	1.8	**35.0, 9.5**
24	41.0	1.3	1.1	**35.0**
25	61.7	1.2	**25.6**	
26	167.7	**15.7**[c]	0.7	
27	203.8	**17.1**	0.7	
28	41.4	1.0	**20.2**	
29	23.1	**15.3**	1.0	
30	28.5	1.3	**21.5**	
31	28.7	**15.4**	1.0	
32	28.9	1.0	**19.6**	
33	28.8	**13.9**	0.8	
34	31.3	0.7	**15.6**	
35	22.1	**13.0**	0.7	
36	14.0	2.2	**50.4**	

[a] The DMSO signal (49.5 ppm) was used as a reference [b] Enrichment ratios (ER) were calculated by comparison to signals from the unlabeled compound [c] Resonances in bold were determined as having been enriched

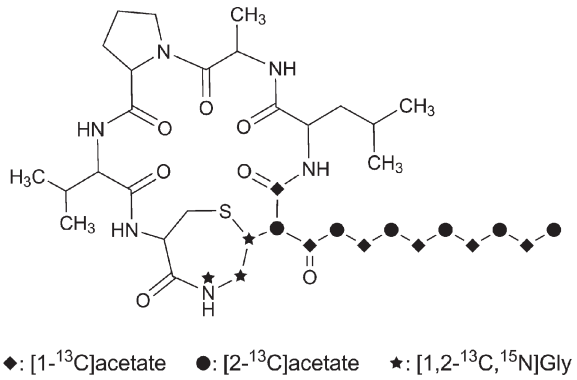

Fig. 4 Incorporation of isotopically labeled [1-^{13}C]acetate, [2-^{13}C] acetate, and [1, 2-^{13}C,^{15}N]glycine in mutanobactin A (**1**).

Previously, we had predicted that the mutanobactins were derived from a hybrid polyketide-nonribosomal-peptide-synthetase pathway.[27] Upon examination of the biosynthetic gene cluster, it was proposed that seven amino acids would be incorporated into the mutanobactins; however, evidence gathered from the chemical analysis of **1** revealed that only six amino acid residues were readily apparent.[28] We speculated that C-26 in **1** and carbon atoms in the immediate vicinity (*i.e.*, C-24, C-25, and/or C-26) may have been derived from the incorporation and subsequent rearrangement of Gly and Asp residues. In order to test this theory, feeding studies were performed utilizing ^{13}C and ^{15}N enriched (>98%) Gly and Asp. We observed that cultures dosed with [1,2-^{13}C,^{15}N]Gly showed significant isotope incorporation at N-23, C-23, and C-24 (Table 2), whereas none of the atoms were labeled when [1,2,3,4-^{13}C,^{15}N]Asp was added (data not shown). These data indicated that Gly is fully integrated into the mutanobactin skeleton while Asp is either not incorporated or latter excised during the biosynthetic process (Fig. 4). Despite these new insights, the origins of C-25 and C-26 in **1** remained unknown. Suspecting that the polyketide synthase could contribute one or both of these carbon atoms, we conducted separate feeding experiments using [1-^{13}C]acetate and [2-^{13}C]acetate. Addition of [1-^{13}C]acetate to the culture medium resulted in substantial enhancement of the NMR signals for C-26, C-27, C-29, C-31, C-33, and C-35 in compound **1** (Table 2 and Fig. 4). In contrast, incorporation of [2-^{13}C]acetate to the growth medium led to enhancement of the NMR resonances for C-25, C-28, C-30, C-32, and C-34 in compound **1** (Table 2 and Fig. 3). Therefore, head-to-tail condensation of six acetate units is believed to be responsible for generating these 12 carbon atoms in the mutanobactin skeleton. We propose that the mutanobactins are generated *via* the sequential addition of L-Leu, L-Ala (later epimerized), L-Pro, L-Val (or L-Ile), L-Cys (or L-Aaba), and L-Gly to the polyketide chain. In view of the structure of metabolite **4**, we suspect that closure of the 20-member macrocycle precedes formation of the 1,4-thiazepan-5-one ring (Fig. S38†). This process may occur by deprotonation of the β-keto amide methylene (C-25, pK_a ~10.8 based on ChemAxon pK_a predictor) to form an enolate anion, which would attack the Gly thioester carbonyl and release the metabolite from the synthetase. Next, formation of the 1,4-thiazepan-5-one ring could proceed *via* either reduction of the C-24 carbonyl followed by nucleophilic attack of the thiol on the secondary alcohol or direct attack of the thiol on the C-24 carbonyl. While these mechanisms present certain challenges and should be regarded with caution, both help illustrate how inflection of the 1,4-thiazepan-5-one ring systems in **1** and **3** may have arisen (Fig. S38†).

We had previously shown that a *S. mutans* mutant lacking the mutanobactin gene cluster was unable to block filament formation of pathogenic *Candida albicans* in a co-culture system.[28] Furthermore, addition of **1** to *C. albicans* under filament promoting conditions suppressed the formation of mycelia. Although the linkage between filament formation and pathogenesis is under debate,[33,34] it is well documented that it is one of several essential steps in *Candida* biofilm formation.[35,36] In clinical settings, yeast are often encountered in polymicrobial biofilm communities.[37,38] While ensconced in biofilms, pathogens such as *C. albicans* have diminished susceptibilities to antibiotics and are challenging targets for *in vivo* elimination.[39,40] We tested **1**–**4** in an assay designed to determine if the mutanobactins could inhibit *C. albicans* biofilm formation. Compound **4** was found to be the most potent inhibitor of biofilm formation with an IC_{50} value of 5.3 ± 0.9 μM (Table 3). In comparison, farnesol, a well-known and widely tested inhibitor of *C. albicans* biofilm formation,[41–43] had a much higher IC_{50} value of 1.4 × 10^2 ± 1.2 μM. Compounds **1** and **2** showed reduced activities with IC_{50} values of 3.4 × 10 ± 1.3 and 9.1 × 10 ± 1.6 μM, respectively. Metabolite **3** showed no activity at concentrations up to 200 μM. The significant impact of C-25 epimerization on the biological activity of this metabolite is quite striking and it suggests insightful discoveries concerning the mutanobactin pharmacophore could be revealed through detailed structure–activity studies. It is also noteworthy that none of the compounds reduced the viability of *C. albicans* (tested over a range from 6.25 to 200 μM), which indicates that the mutanobactins may selectively exert their inhibitory effects against a biofilm-formation-specific target (*e.g.*, filament formation).

Table 3 Biofilm formation inhibition and MIC values of metabolites **1–4** and farnesol against *C.albicans* Day185

Compound	Biofilm formation inhibition (IC_{50} ± SD in μM)[a]	Growth inhibition (MIC in μM)
1	3.4 × 10 ± 1.3	>200
2	9.1 × 10 ± 1.6	>200
3	>200	>200
4	5.3 ± 0.9	>200
Farnesol	1.4 × 10^2 ± 1.2	>200

[a] IC_{50} are expressed as the concentration of compound required to cause a 50% reduction in biofilm formation

Conclusions

The human microbiome contains an abundance of taxonomically diverse bacteria, a number of which have the potential to generate secondary metabolites. It is reasonable to expect that many of these microbiome-derived compounds will have evolved unique biological functions that make them important factors for maintaining our wellbeing. The mutanobactins provide a foretaste of the intriguing roles and potential therapeutic applications of compounds biosynthesized by bacteria living in and on the human body.

Experimental section

General experimental procedures

Optical rotations were measured on a Rudolph Research Autopol III automatic polarimeter. UV data were measured on Hewlett Packard 8452A diode array spectrophotometer, IR was measured on A2 Technology Nano FTIR. NMR data were obtained on Varian VNMR spectrometers (500 MHz for ^{1}H, 100 MHz for ^{13}C) with broad band and triple resonance probes at 20 ± 0.5 °C. LC-ESIMS data were collected using a Thermo-Finnigan Surveyor LC system and a Finnigan LCQ Deca mass analyzer. HRESIMS data were obtained by electrospray ionization employing an Agilent 6538 UHD Accurate-Mass Quadrupole TOF mass analyzer. HPLC separations were performed on a Shimadzu system using a SCL-10A VP system controller and Gemini 5 μm C_{18} column, (110 Å, 250 × 21.2 mm) with flow rates of 1 to 10 mL min^{-1}. All solvents were of ACS grade or better.

Fermentation, extraction, and purification of mutanobactins

Streptococcus mutans UA159 was prepared by inoculating 40 L of brain-heart infusion (BHI) broth with 100 mL of an overnight stationary *S. mutans* UA159 culture. The culture was incubated under microoxic conditions at 37 °C for 96 h. The culture was extracted three times with equal volumes of ethyl acetate, which was evaporated *in vacuo* to generate the *S. mutans* UA159 extract. The crude extract (35 g) was separated into five fractions by HP20SS column chromatography (step gradient of 30%, 50%, 70%, 90%, and 100% MeOH in H_2O). Fractions Fr.4 (824 mg) and Fr.5 (156 mg) were combined (named Fr.7) and further separated into seven subfractions by preparative reversed-phase HPLC (eluted with a linear gradient of 20% to 100% MeOH in H_2O, 10.0 mL min^{-1}). Subfraction Fr.7-5 was subjected to repeated semi-preparative reversed-phase HPLC (isocratic 85% MeOH in H_2O followed by 70% CH_3CN in H_2O, 4.0 mL min^{-1}) to provide **1** (52.7 mg, 0.15% yield), **2** (5.4 mg, 0.015% yield), **3** (34.6 mg, 0.098% yield), and **4** (2.4 mg, 0.0069% yield).

Biofilm and growth inhibition assays with *C. albicans*

The effects of mutanobactins on the growth of *C.albicans* DAY185 were tested using the methods prescribed in the CLSI guidelines.[44] The biofilm inhibition assay was performed as described by Chandra *et al.*[45] with the following modifications. The *C. albicans* strain DAY185 was cultured in BHI medium (Becton Dickinson, USA) at 37 °C overnight and washed with sterile PBS buffer (pH 7.4, EMD Chemicals Inc., USA), and resuspended in RPMI 1640 medium (Sigma Chemical Corp., USA) buffered to pH 7.0 with MOPS (3-(*N*-morpholino)propanesulfonic acid, 0.165 M). Test compounds were prepared in DMSO at a final concentration of 20 mM and were serially diluted in 2-fold steps with RPMI 1640 plus MOPS medium from the highest concentration of 200 μM. Farnesol was used as a positive control.[46] One hundred microlitres of yeast suspension (2.5 × 10^3 cells mL^{-1}) were added to the wells of a 96-well microplate (Costar 3370, Corning Inc., USA) containing the diluted compounds (from 200 μM to 6.25 μM) or DMSO (v/v 1%) and the plate incubated at 37 °C. After 48 h, yeast viability was measured by XTT assay.[47] Briefly, yeast cells were treated with 0.1 mg mL^{-1} XTT at 37 °C for 1 h. The absorbance was taken at 490 nm using a microplate reader (Infinite M200, Tecan Group Ltd., Switzerland). The minimum inhibitory concentration (MIC) for growth was defined as the lowest concentration that caused ≥80% reduction in the metabolic activity of the yeast. After the initial XTT assay was completed, the medium was immediately aspirated from each well and the wells washed twice with sterile PBS to remove nonadherent cells. Aliquots consisting of 100 μL RPMI 1640 plus MOPS medium were then added to each well. The washed biofilms were again measured using the XTT assay. All experiments were performed in triplicate on three separate occasions. The 50% inhibitory concentration (IC_{50}) values for biofilm inhibition were calculated using GraphPad Prism software (GraphPad, USA).

Feeding experiments with isotopically labeled acetate and amino acids

For the isotope labeling experiments, 500 mg of [1-^{13}C] or [2-^{13}C]sodium acetate, or 100 mg [1,2-^{13}C,^{15}N]Gly or [1,2,3,4-^{13}C,^{15}N]Asp (Cambridge Isotope Laboratories, Inc., USA) were dissolved in water and filter sterilized. The isotopes were added separately to 6 L batches of sterile BHI medium and culture vessels inoculated with overnight cultures of *S. mutans*. Cultures were maintained at 37 °C for 86 h at which time they were extracted with equal volumes of EtOAc (3×). The extracts were each separated into three fractions over silica gel using an Isolera flash column. The fractions containing mutanobactins were further purified by preparative-HPLC and semi-preparative

HPLC to give approximately 5 mg of labeled **1** from each of the three cultures. A ^{13}C NMR spectrum was obtained at 100 MHz for each of the labeled compounds under identical experimental conditions.

Mutanobactin B (2). White amorphous powder, $[\alpha]_D^{21}$ 24.4 (*c* 0. 27, MeOH); UV (MeOH) λ_{max} (log ε) 204 (3.17) nm; IR ν_{max} 3300, 3250, 2960, 2920, 2850, 1640 cm^{-1}; ^1H and ^{13}C NMR data, see Table 1; HRESIMS *m*/*z* 757.4298 $[M + Na]^+$ (calcd for $C_{37}H_{62}N_6O_7SNa$,757.4298).

Mutanobactin C (3). White amorphous powder, $[\alpha]_D^{21}$ −3.7 (*c* 0. 38, MeOH); UV (MeOH) λ_{max} (log ε) 204 (4.38) nm; IR ν_{max} 3280, 2960, 2920, 2850, 1640 cm^{-1}; ^1H and ^{13}C NMR data, see Table 1; HRESIMS *m*/*z* 743.4138 $[M + Na]^+$ (calcd for $C_{36}H_{60}N_6O_7SNa$, 743.4142).

Mutanobactin D (4). White amorphous powder, $[\alpha]_D^{21}$ 18.3 (*c* 0. 12, MeOH); UV (MeOH) λ_{max} (log ε) 204 (4.29); IR ν_{max} 3290, 2960, 2920, 2850, 1640 cm^{-1}; ^1H and ^{13}C NMR data, see Table 1; HRESIMS *m*/*z* 743.4681 $[M + Na]^+$ (calcd for $C_{37}H_{64}N_6O_8Na$, 743.4683).

Acknowledgements

Financial support for this project was provided in part by a Challenge Grant from the Office of the Vice President for Research, University of Oklahoma, Norman Campus and an award through the Shimadzu Equipment Grant Program. We are grateful to C. A. Kumamoto and A. Mitchell for kindly providing *C. albicans* DAY185. We thank F. Qi for the *S. mutans* UA159 culture.

References

1 L. M. C. Collins and C. Dawes, *J. Dent. Res.*, 1987, **66**, 1300–1302.
2 G. Xie, P. S. G. Chain, C. C. Lo, K. L. Liu, J. Gans, J. Merritt and F. Qi, *Molecular Oral Microbiology*, 2010, **25**, 391–405.
3 E. Zaura, B. Keijser, S. Huse and W. Crielaard, *BMC Microbiol.*, 2009, **9**, 259.
4 I. Nasidze, J. Li, D. Quinque, K. Tang and M. Stoneking, *Genome Res.*, 2009, **19**, 636–643.
5 V. Lazarevic, K. Whiteson, D. Hernandez, P. Francois and J. Schrenzel, *BMC Genomics*, 2010, **11**, 523.
6 F. E. Dewhirst, T. Chen, J. Izard, B. J. Paster, A. C. R. Tanner, W. H. Yu, A. Lakshmanan and W. G. Wade, *J. Bacteriol.*, 2010, **192**, 5002–5017.
7 B. J. F. Keijser, E. Zaura, S. M. Huse, J. M. B. M. van der Vossen, F. H. J. Schuren, R. C. Montijn, J. M. ten Cate and W. Crielaard, *J. Dent. Res.*, 2008, **87**, 1016–1020.
8 J. Ahn, L. Yang, B. J. Paster, I. Ganly, L. Morris, Z. Pei and R. B. Hayes, *PLoS One*, 2011, **6**, e22788.
9 M. A. Ghannoum, R. J. Jurevic, P. K. Mukherjee, F. Cui, M. Sikaroodi, A. Naqvi and P. M. Gillevet, *PLoS Pathog.*, 2010, **6**, e1000731.
10 F. Maruyama, M. Kobata, K. Kurokawa, K. Nishida, A. Sakurai, K. Nakano, R. Nomura, S. Kawabata, T. Ooshima, K. Nakai, M. Hattori, S. Hamada and I. Nakagawa, *BMC Genomics*, 2009, **10**, 358.
11 D. Ajdić, W. M. McShan, R. E. McLaughlin, G. Savić, J. Chang, M. B. Carson, C. Primeaux, R. Tian, S. Kenton, H. Jia, S. Lin, Y. Qian, S. Li, H. Zhu, F. Najar, H. Lai, J. White, B. A. Roe and J. J. Ferretti, *Proc. Natl. Acad. Sci. U. S. A.*, 2002, **99**, 14434–14439.
12 J. Kreth, J. Merritt and F. Qi, *DNA Cell Biol.*, 2009, **28**, 397–403.
13 J. A. Lemos and R. A. Burne, *Microbiology*, 2008, **154**, 3247–3255.
14 H. K. Kuramitsu, X. He, R. Lux, M. H. Anderson and W. Shi, *Microbiol. Mol. Biol. Rev.*, 2007, **71**, 653–670.
15 J. A. Aas, A. L. Griffen, S. R. Dardis, A. M. Lee, I. Olsen, F. E. Dewhirst, E. J. Leys and B. J. Paster, *J. Clin. Microbiol.*, 2008, **46**, 1407–1417.
16 P. Belda-Ferre, L. D. Alcaraz, R. Cabrera-Rubio, H. Romero, A. Simon-Soro, M. Pignatelli and A. Mira, *ISME J.*, 2012, **6**, 46–56.
17 T. Pereira-Cenci, D. M. Deng, E. A. Kraneveld, E. M. M. Manders, A. A. Del Bel Cury, J. M. ten Cate and W. Crielaard, *Arch. Oral Biol.*, 2008, **53**, 755–764.
18 R. Vílchez, A. Lemme, B. Ballhausen, V. Thiel, S. Schulz, R. Jansen, H. Sztajer and I. Wagner-Döbler, *ChemBioChem*, 2010, **11**, 1552–1562.
19 M. B. Zeisel, V. A. Druet, J. Sibilia, J.-P. Klein, V. Quesniaux and D. Wachsmann, *J. Immunol.*, 2005, **174**, 7393–7397.
20 F. Berlutti, A. Catizone, G. Ricci, A. Frioni, T. Natalizi, P. Valenti and A. Polimeni, *Int. J. Immunopathol. Pharmacol.*, 2010, **23**, 1253–1260.
21 J. M. Crawford and J. Clardy, *Chem. Commun.*, 2011, **47**, 7559–7566.
22 P. E. Kolenbrander, R. J. Palmer, S. Periasamy and N. S. Jakubovics, *Nat. Rev. Microbiol.*, 2010, **8**, 471–480.
23 N. S. Jakubovics, *Molecular Oral Microbiology*, 2010, **25**, 4–14.
24 J. Y. Yang, J. R. Karr, J. D. Watrous and P. C. Dorrestein, *Curr. Opin. Chem. Biol.*, 2011, **15**, 79–87.
25 J. L. Sonnenburg and M. A. Fischbach, *Sci. Transl. Med.*, 2011, **3**, 78ps12.
26 M. Zimmermann and M. A. Fischbach, *Chem. Biol.*, 2010, **17**, 925–930.
27 C. Wu, R. Cichewicz, Y. Li, J. Liu, B. Roe, J. Ferretti, J. Merritt and F. Qi, *Appl. Environ. Microbiol.*, 2010, **76**, 5815–5826.
28 P. M. Joyner, J. Liu, Z. Zhang, J. Merritt, F. Qi and R. H. Cichewicz, *Org. Biomol. Chem.*, 2010, **8**, 5486–5489.
29 D. W. Williams, T. Kuriyama, S. Silva, S. Malic and M. A. O. Lewis, *Periodontology 2000*, 2011, **55**, 250–265.
30 M. D. LaFleur, Q. Qi and K. Lewis, *Antimicrob. Agents Chemother.*, 2010, **54**, 39–44.
31 M. D. LaFleur, C. A. Kumamoto and K. Lewis, *Antimicrob. Agents Chemother.*, 2006, **50**, 3839–3846.
32 R. Bhushan and H. Brückner, *Amino Acids*, 2004, **27**, 231–247.
33 S. M. Noble, S. French, L. A. Kohn, V. Chen and A. D. Johnson, *Nat. Genet.*, 2010, **42**, 590–598.
34 P. L. Carlisle, M. Banerjee, A. Lazzell, C. Monteagudo, J. L. López-Ribot and D. Kadosh, *Proc. Natl. Acad. Sci. U. S. A.*, 2009, **106**, 599–604.
35 B. B. Fuchs, J. Eby, C. J. Nobile, J. B. El Khoury, A. P. Mitchell and E. Mylonakis, *Microbes Infect.*, 2010, **12**, 488–496.
36 G. Ramage, K. VandeWalle, J. L. López-Ribot and B. L. Wickes, *FEMS Microbiol. Lett.*, 2002, **214**, 95–100.
37 A. Y. Peleg, D. A. Hogan and E. Mylonakis, *Nat. Rev. Microbiol.*, 2010, **8**, 340–349.
38 M. E. Shirtliff, B. M. Peters and M. A. Jabra-Rizk, *FEMS Microbiol. Lett.*, 2009, **299**, 1–8.
39 C. J. Seneviratne, L. J. Jin, Y. H. Samaranayake and L. P. Samaranayake, *Antimicrob. Agents Chemother.*, 2008, **52**, 3259–3266.
40 P. K. Mukherjee and J. Chandra, *Drug Resist. Updates*, 2004, **7**, 301–309.
41 K. W. Nickerson, A. L. Atkin and J. M. Hornby, *Appl. Environ. Microbiol.*, 2006, **72**, 3805–3813.
42 G. Ramage, S. P. Saville, B. L. Wickes and J. L. Lopez-Ribot, *Appl. Environ. Microbiol.*, 2002, **68**, 5459–5463.
43 K. Weber, B. Schulz and M. Ruhnke, *Yeast*, 2010, **27**, 727–739.
44 Clinical and Laboratory Standards Institute, *Reference Method for Broth Dilution Antifungal Susceptibility Testing of Yeasts - Approved Standard (CLSI document M27-A3)*, 3rd edn, 2008.
45 J. Chandra, P. K. Mukherjee and M. A. Ghannoum, *Nat. Protoc.*, 2008, **3**, 1909–1924.
46 A. Deveau and D. A. Hogan, in *Quorum Sensing Methods and Protocols. Part II. Determining the Function of Autoinducers In vivo*, ed. K. P. Rumbaugh, Humana Press (Springer), New York, 2011, 692, 219–233.
47 J. E. Nett, M. T. Cain, K. Crawford and D. R. Andes, *J. Clin. Microbiol.*, 2011, **49**, 1426–1433.

